Influence of Defects on the Electrical Characteristics of Mercury-Drop Junctions: Self-Assembled Monolayers of *n*-Alkanethiolates on Rough and Smooth Silver

Emily A. Weiss,[#] Ryan C. Chiechi,[#] George K. Kaufman,[#] Jennah K. Kriebel,[#] Zhefeng Li,[#] Marco Duati,[§] Maria A. Rampi,[§] and George M. Whitesides*,[#]

Contribution from the Department of Chemistry and Chemical Biology, Harvard University, 12 Oxford Street, Cambridge, Massachusetts 02138, and Dipartimento di Chimica, Università di Ferrara, Via L. Borsari 46, Ferrara 44100, Italy

Received November 4, 2006; E-mail: gwhitesides@gmwgroup.harvard.edu

Abstract: This paper compares the structural and electrical characteristics of self-assembled monolayers (SAMs) of *n*-alkanethiolates, SC_n ($n = 10, 12, 14$), on two types of silver substrates: one used as-deposited (AS-DEP) by an electron-beam evaporator, and one prepared using the method of template-stripping. Atomic force microscopy showed that the template-stripped (TS) silver surfaces were smoother and had larger grains than the AS-DEP surfaces, and reflectance−absorbance infrared spectroscopy showed that SAMs formed on TS substrates were more crystalline than SAMs formed on AS-DEP substrates. The range of current densities, J (A/cm^2), measured through mercury-drop junctions incorporating a given SAM on AS-DEP silver was, on average, several orders of magnitude larger than the range of J measured through the same SAM on TS silver, and the AS-DEP junctions failed, on average, 3.5 times more often within five current density−voltage (J−V) scans than did TS junctions (depending on the length of the alkyl chains of the molecules in the SAM). The apparent log-normal distribution of J through the TS junctions suggests that, in these cases, it is the variability in the effective thickness of the insulating layer (the distance the electron travels between electrodes) that results in the uncertainty in J. The parameter describing the decay of current density with the thickness of the insulating layer, β, was either 0.57 Å^{-1} at $V = +0.5$ V (calculated using the log-mean of the distribution of values of J) or 0.64 Å^{-1} (calculated using the peak of the distribution of values of J) for the TS junctions; the latter is probably the more accurate. The mechanisms of failure of the junctions, and the degree and sources of uncertainty in current density, are discussed with respect to a variety of defects that occur within Hg-drop junctions incorporating SAMs on silver.

Introduction

This paper compares the structural and electrical characteristics of self-assembled monolayers (SAMs) of *n*-alkanethiolates on two types of silver substrates:[1−4] one using silver films as-deposited (AS-DEP) by an electron-beam evaporator,[5,6] and one using silver films prepared by the method of template-stripping.[7−11] We demonstrate that the method used to fabricate thin metallic substrates affects both the structure of the metal−organic interface and the intermolecular organization within the SAM.[3,7−9,12−17] The template-stripped (TS) silver substrates were flatter, and had larger grains, than the AS-DEP substrates. We measured the current density−voltage (J−V) characteristics of bilayer junctions comprising a SAM of *n*-alkanethiolates on Ag in contact with a SAM of *n*-alkanethiolates supported on an Hg electrode. During measurements, the entire junction was immersed in a solution of alkanethiol in hexadecane. As previously,[18−21] we call this junction a "mercury-drop junction". Unlike most previous experimental procedures, in this study, we prepared the SAMs on the silver and mercury electrodes

[#] Harvard University.
[§] Università di Ferrara.

(1) Follonier, S.; Miller, W. J. W.; Abbott, N. L.; Knoesen, A. *Langmuir* **2003**, *19*, 10501.
(2) Bertilsson, L.; Liedberg, B. *Langmuir* **1993**, *9*, 141.
(3) Laibinis, P. E.; Whitesides, G. M.; Allara, D. L.; Tao, Y. T.; Parikh, A. N.; Nuzzo, R. G. *J. Am. Chem. Soc.* **1991**, *113*, 7152.
(4) Gupta, P.; Ulman, A.; Fanfan, S.; Korniakov, A.; Loos, K. *J. Am. Chem. Soc.* **2005**, *127*, 4.
(5) Levlin, M.; Laakso, A. *Appl. Surf. Sci.* **2001**, *171*, 257.
(6) Dumont, J.; Wiame, F.; Ghijsen, J.; Sporken, R. *Surf. Sci.* **2004**, *572*, 459.
(7) Gupta, P.; Loos, K.; Korniakov, A.; Spagnoli, C.; Cowman, M.; Ulman, A. *Angew. Chem., Int. Ed.* **2004**, *43*, 520.
(8) Ragan, R.; Ohlberg, D.; Blackstock, J. J.; Kim, S.; Williams, R. S. *J. Phys. Chem. B* **2004**, *108*, 20187.
(9) Samori, P.; Diebel, J.; Loewe, H.; Rabe, J. P. *Langmuir* **1999**, *15*, 2592.
(10) Wagner, P.; Hegner, M.; Guntherodt, H.-J.; Semenza, G. *Langmuir* **1995**, *11*, 3867.
(11) Naumann, R.; Schiller, S. M.; Gless, F.; Grohe, B.; Hartman, K. B.; Karcher, I.; Koper, I.; Lubben, J.; Vasilev, K.; Knoll, W. *Langmuir* **2003**, *19*, 5435.

(12) Love, J. C.; Estroff, L. A.; Kriebel, J. K.; Nuzzo, R. G.; Whitesides, G. M. *Chem. Rev.* **2005**, *105*, 1103.
(13) Yang, G.; Liu, G.-Y. *J. Phys. Chem. B* **2003**, *107*, 8746.
(14) Poirier, G. E.; Pylant, E. D. *Science* **1996**, *272*, 1145.
(15) Yamada, R.; Wano, H.; Uosaki, K. *Langmuir* **2000**, *16*, 5523.
(16) Laffineur, F.; Couturier, N.; Delhalle, J.; Mekhalif, Z. *Appl. Surf. Sci.* **2003**, *212−213*, 452.
(17) Selzer, Y.; Salomon, A.; Cahen, D. *J. Am. Chem. Soc.* **2002**, *124*, 2886.
(18) Rampi, M. A.; Whitesides, G. M. *Chem. Phys.* **2002**, *281*, 373.
(19) Tran, E.; Grave, C.; Whitesides, G. A.; Rampi, M. A. *Electrochim. Acta* **2005**, *50*, 4850.
(20) Holmlin, R. E.; Ismagilov, R. F.; Haag, R.; Mujica, V.; Ratner, M. A.; Rampi, M. A.; Whitesides, G. M. *Angew. Chem., Int. Ed.* **2001**, *40*, 2316.
(21) Holmlin, R. E.; Haag, R.; Chabinyc, M. L.; Ismagilov, R. F.; Cohen, A. E.; Terfort, A.; Rampi, M. A.; Whitesides, G. M. *J. Am. Chem. Soc.* **2001**, *123*, 5075.

within a single junction from the same *n*-alkanethiol (that is, the two SAMs formed a compositionally symmetric bilayer). We used this configuration so that, in principle, the molecules in solution could "repair" pinholes and other defects in the SAMs and could exchange with molecules in the SAMs without forming mixed monolayers.[22−24] Template-stripped Ag films proved to be better substrates for the electrical characterization of SAMs of *n*-alkanethiolates than did AS-DEP Ag films in two important ways: (i) The range of *J* through the junctions with TS surfaces ("TS junctions") was $10^2−10^4$ times smaller (depending on the length of the alkyl chain) than that through junctions incorporating AS-DEP surfaces ("AS-DEP junctions"). (ii) The AS-DEP junctions failed (by amalgamation of the Ag and Hg electrodes), on average, 4.6 times more often during traces 1−3, and 3.5 times more often during traces 1−5, than did TS junctions (where a trace is a *J*−*V* scan, with *V* = 0 V → 0.5 V → −0.5 V → 0 V, in steps of 0.05 V).

The Single-Barrier Model for Tunneling through Insulating SAMs. A number of studies have concluded—based on the observed exponential decrease of the current density with increasing distance between electrodes[25−27]—that the predominant mechanism of charge transport through a SAM of an *n*-alkanethiolate in a metal−insulator−metal (MIM) junction is non-resonant superexchange tunneling. A simple way to model the distance dependence of charge transport through a MIM junction that displays such behavior is to consider the insulating portion of the junction to be a rectangular tunneling barrier (eqs 1). Here, *J* (the current density), J_0, and j_0 have units of A/cm².

$$J = J_0\, e^{-\beta d} \qquad (1a)$$

$$J_0 = j_0\, e^{-\alpha d_0} \qquad (d, d_0 \geq 0) \qquad (1b)$$

To apply this model, we partition the insulating layer into a portion whose thickness (d_0, Å) is constant and a portion whose thickness (*d*, Å) changes as the molecular structure of the insulating layer varies. A plot of ln *J* vs *d* has a *y*-intercept ln J_0 and slope $-\beta$ (Å⁻¹); this slope quantifies the decay of the tunneling probability with increasing *d*. The value of β does not depend on the choice of d_0. The value of J_0 depends on three parameters (eq 1b): (i) j_0, the current density that would flow through the junction in the hypothetical case that the two metals were in contact but still electrically isolated (i.e., if the thickness of the insulating layer were zero), (ii) d_0, and (iii) α, the characteristic decay of the tunneling probability with increasing values of d_0. The factor $\exp(-\alpha d_0)$ is sometimes called the "contact resistance" because it quantifies the characteristics (height, length) of the tunneling barrier that the electron encounters at the interface between the metal and the insulator.[28,29] In studying bilayer junctions, we also include in

this factor the tunneling barrier that the electron encounters at the van der Waals interface between the two SAMs (the SAM// SAM interface).[30,31] The contact resistance thus includes all the interfacial terms. We cannot independently evaluate these terms (using the kinds of experiments we describe in this paper), but we believe they are roughly constant for all the junctions we have studied within a class (TS and AS-DEP) and independent of the length of the alkyl group.

An electron, in principle, tunnels through a junction via multiple pathways: some that follow the carbon backbone of the molecule, and some that involve multiple molecules. The respective contributions of intermolecular and intramolecular charge transport are believed to (but have not been unambiguously proven to) depend heavily on the tilt angle of the alkanethiolate molecules with respect to the metal substrate.[26,32] For close-packed SAMs of *n*-alkanethiolates on Ag and Hg, in which the molecules have tilt angles of ∼10° and ∼0°, respectively,[33−35] the magnitude of the tunneling current appears to correlate with the molecular length—that is, the distance between the electrodes along the molecular axis—and not with the average shortest physical distance between the electrodes.

Uncertainty in the Measurements of Current Density through MIM Junctions. Self-assembled monolayers of *n*-alkanethiolates are the insulating layer for many MIM junctions, including those with one thin-film metal electrode and one conducting tip, such as the tip of a conducting probe atomic force microscope (CP-AFM)[27,29,36] or a scanning tunneling microscope (STM),[13−15,37−39] those with two thin-film metal electrodes,[13,40−43] and those with at least one liquid-metal electrode (Hg-drop junctions).[18−21,26,35,44−53] In some of these studies, the electrode contacts a large number (∼1 × 10¹²) of

(22) Chung, C.; Lee, M. *J. Electroanal. Chem.* **1999**, *468*, 91.
(23) Nishida, N.; Hara, M.; Sasabe, H.; Knoll, W. *Jpn. J. Appl. Phys. Part 1* **1997**, *36*, 2379.
(24) Baralia Gabriel, G.; Duwez, A.-S.; Nysten, B.; Jonas Alain, M. *Langmuir* **2005**, *21*, 6825.
(25) Lee, T.; Wang, W.; Klemic, J. F.; Zhang, J. J.; Su, J.; Reed, M. A. *J. Phys. Chem. B* **2004**, *108*, 8742.
(26) Slowinski, K.; Chamberlain, R. V.; Miller, C. J.; Majda, M. *J. Am. Chem. Soc.* **1997**, *119*, 11910.
(27) Salomon, A.; Cahen, D.; Lindsay, S.; Tomfohr, J.; Engelkes, V. B.; Frisbie, C. D. *Adv. Mater.* **2003**, *15*, 1881.
(28) Bihary, Z.; Ratner, M. A. *Phys. Rev. B* **2005**, *72*, 115439/1.
(29) Engelkes, V. B.; Beebe, J. M.; Frisbie, C. D. *J. Am. Chem. Soc.* **2004**, *126*, 14287.
(30) The length (along the C−C backbone) of two *trans*-extended alkyl chains, each with *n* carbon atoms, whose terminal methyl groups associate at a van der Waals interface is ∼2.5 Å greater than that of one *trans*-extended alkyl chain with 2*n* carbon atoms.
(31) Steiner, T.; Desiraju, G. R. *Chem. Commun.* **1998**, 891.
(32) Yamamoto, H.; Waldeck, D. H. *J. Phys. Chem. B* **2002**, *106*, 7469.
(33) Magnussen, O. M.; Ocko, B. M.; Duetsch, M.; Regan, M. J.; Pershan, P. S.; Abernathy, D.; Gurebel, G.; Legrand, J.-F. *Nature* **1996**, *384*, 250.
(34) Lavrich, D. J.; Wetterer, S. M.; Bernasek, S. L.; Scoles, G. *J. Phys. Chem. B* **1998**, *102*, 3456.
(35) Demoz, A.; Harrison, D. J. *Langmuir* **1993**, *9*, 1046.
(36) Beebe, J. M.; Engelkes, V. B.; Miller, L. L.; Frisbie, C. D. *J. Am. Chem. Soc.* **2002**, *124*, 11268.
(37) Dunbar, T. D.; Cygan, M. T.; Bumm, L. A.; McCarty, G. S.; Burgin, T. P.; Reinerth, W. A.; Jones, L., II; Jackiw, J. J.; Tour, J. M.; Weiss, P. S.; Allara, D. L. *J. Phys. Chem. B* **2000**, *104*, 4880.
(38) Dameron, A. A.; Ciszek, J. W.; Tour, J. M.; Weiss, P. S. *J. Phys. Chem. B* **2004**, *108*, 16761.
(39) Xu, B.; Tao, N. J. *Science* **2003**, *301*, 1221.
(40) Akkerman, H. B.; Blom, P. W. M.; de Leeuw, D. M.; de Boer, B. *Nature* **2006**, *441*, 69.
(41) Wang, W. Y.; Lee, T.; Reed, M. A. *J. Phys. Chem. B* **2004**, *108*, 18398.
(42) Haick, H.; Ambrico, M.; Ghabboun, J.; Ligonzo, T.; Cahen, D. *Phys. Chem. Chem. Phys.* **2004**, *6*, 4538.
(43) Wang, W.; Lee, T.; Reed, M. A. *Phys. Rev. B* **2003**, *68*, 035416/1.
(44) Chabinyc, M. L.; Chen, X. X.; Holmlin, R. E.; Jacobs, H.; Skulason, H.; Frisbie, C. D.; Mujica, V.; Ratner, M. A.; Rampi, M. A.; Whitesides, G. M. *J. Am. Chem. Soc.* **2002**, *124*, 11730.
(45) Grave, C.; Tran, E.; Samori, P.; Whitesides, G. M.; Rampi, M. A. *Synth. Met.* **2004**, *147*, 11.
(46) Slowinski, K.; Slowinska, K. U.; Majda, M. *J. Phys. Chem. B* **1999**, *103*, 8544.
(47) Salomon, A.; Arad-Yellin, R.; Shanzer, A.; Karton, A.; Cahen, D. *J. Am. Chem. Soc.* **2004**, *126*, 11648.
(48) Galperin, M.; Nitzan, A.; Sek, S.; Majda, M. *J. Electroanal. Chem.* **2003**, *550−551*, 337.
(49) Slowinski, K.; Majda, M. *J. Electroanal. Chem.* **2000**, *491*, 139.
(50) Ocko, B. M.; Kraack, H.; Pershan, P. S.; Sloutskin, E.; Tamam, L.; Deutsch, M. *Phys. Rev. Lett.* **2005**, *94*, 017802.
(51) Sek, S.; Bilewicz, R.; Slowinski, K. *Chem. Commun.* **2004**, 404.
(52) York, R. L.; Nguyen, P. T.; Slowinski, K. *J. Am. Chem. Soc.* **2003**, *125*, 5948.
(53) York, R. L.; Nacionales, D.; Slowinski, K. *Chem. Phys.* **2005**, *319*.

Table 1. Current Density (J) through Hg-Drop Junctions with SAMs of SC_n

$N_C{}^a$	junction	method^b	V^c (V)	J (A/cm²)	log($J_{max}/J_{min})^d$	ref
9	Ag-SC₉S-Hg	AS-DEP	0.4	90.0	0.9	51
	Ag-SC₉SH//Hg	AS-DEP	0.4	12.2		51
	Hg-SC₉//Hg	n/a	0.4	54.6		52
10	Ag-SC₁₀//Hg	AS-DEP	0.4	20.1	0.2	51
	Hg-SC₁₀//Hg	n/a	0.4	33.1		52
11	Hg-SC₁₁//Hg	n/a	0.4	12.2	n/a	52
12	Ag-SC₁₂//Hg	AS-DEP	0.4	1.6	0.9	51
	Ag-SC₁₂S-Hg	AS-DEP	0.4	4.5		51
	Ag-SC₁₂SH//Hg	AS-DEP	0.4	0.61		51
	Hg-SC₁₂//Hg	n/a	0.4	2.7		52
14	Ag-SC₁₄//Hg	AS-DEP	0.4	0.61	n/a	51
15	Ag-SC₁₅//Hg	AS-DEP	0.4	0.37	0.2	51
	Hg-SC₁₅//Hg	n/a	0.4	0.22		52
16	Ag-SC₁₆//Hg	AS-DEP	0.4	0.05	0.7	51
	Hg-SC₁₆//Hg	n/a	0.4	0.03		52
	Hg-SC₈//C₈S-Hg	n/a	0.4	0.14		52
18	Ag-SC₁₈//Hg	AS-DEP	0.4	4.1×10^{-3}	0.4	51
	Hg-SC₁₈//Hg	n/a	0.4	4.1×10^{-3}		52
	Hg-SC₉//C₉S-Hg	n/a	0.4	0.01		52
	Hg-SC₉//C₉S-Hg	n/a	−1.5	3.7×10^{-5}		54
19	Hg-SC₉//C₁₀S-Hg	n/a	−1.5	1.0×10^{-5}	n/a	54
20	Ag-SC₂₀S-Hg	AS-DEP	0.4	0.01	1.9	51
	Ag-SC₂₀SH//Hg	AS-DEP	0.4	1.2×10^{-4}		51
	Ag-SC₁₀//C₁₀S-Hg	TS	0.5	4.3×10^{-4}		TW^e
	Hg-SC₁₀//C₁₀S-Hg	n/a	0.4	2.4×10^{-3}		52
	Hg-SC₁₀//C₁₀S-Hg	n/a	−1.5	6.1×10^{-6}		54
22	Hg-SC₁₁//C₁₁S-Hg	n/a	0.4	3.4×10^{-4}	n/a	52
	Hg-SC₁₁//C₁₁S-Hg	n/a	−1.5	1.4×10^{-6}		54
	Hg-SC₁₀//C₁₂S-Hg	n/a	−1.5	8.3×10^{-7}		54
24	Ag-SC₈//C₁₆S-Hg	AS-DEP	0.5	1.0×10^{-6}	1.6	21
	Ag-SC₁₀//C₁₄S-Hg	AS-DEP	0.5	5.0×10^{-6}		21
	Ag-SC₁₂//C₁₂S-Hg	AS-DEP	0.5	8.0×10^{-6}		21
	Ag-SC₁₂//C₁₂S-Hg	TS	0.5	4.1×10^{-5}		TW^e
	Hg-SC₁₂//C₁₂S-Hg	n/a	0.4	2.8×10^{-5}		52
	Hg-SC₁₂//C₁₂S-Hg	n/a	−1.5	2.1×10^{-7}		54
	Hg-SC₁₀//C₁₄S-Hg	n/a	−1.5	7.5×10^{-8}		54
26	Ag-SC₁₀//C₁₆S-Hg	AS-DEP	0.5	4.0×10^{-7}	n/a	21
	Hg-SC₁₂//C₁₄S-Hg	n/a	−1.5	3.4×10^{-8}		54
28	Ag-SC₁₂//C₁₆S-Hg	AS-DEP	0.5	5.0×10^{-8}	1.4	21
	Ag-SC₁₄//C₁₄S-Hg	TS	0.5	1.4×10^{-6}		TW^e
	Hg-SC₁₄//C₁₄S-Hg	n/a	−1.5	6.2×10^{-9}		54
	Hg-SC₁₂//C₁₆S-Hg	n/a	−1.5	5.6×10^{-9}		54
30	Ag-SC₁₄//C₁₆S-Hg	AS-DEP	0.5	4.0×10^{-9}	n/a	21
32	Ag-SC₁₆//C₁₆S-Hg	AS-DEP	0.5	2.0×10^{-10}	n/a	21

^{a} N_C is the total number of carbons separating the electrodes (see the column labeled "junction" for the composition of the insulating layer). ^{b} The method used to form the (non-mercury) metal substrate; we describe AS-DEP and TS in the text. ^{c} The applied voltage at which J was recorded. ^{d} For a group of junctions with the same value of N_C, the range (in powers of 10) of J values, log(Max/Min) = (log of the maximum value of J) − (log of the minimum value of J). The values of J measured at $V = −1.5$ V^{54} are not included in this calculation. ^{e} These data are from this work. n/a = not applicable.

molecules; in others, it contacts one or a few molecules. The discussion of J allows some level of comparison of charge transport through junctions with different contact areas.

Electrical measurements on MIM junctions with SAMs of *n*-alkanethiolates yield a wide range (greater than 10⁴) of averaged values for J for a given thickness of the SAM; these values do not follow an obvious trend based on the type of metal electrode, metal−molecule interface, or experimental technique.[25,27] The data obtained using Hg-drop junctions seem internally more consistent than the larger set that includes both Hg-drop junctions and other types of junctions (CP-AFM, break junctions, etc.).[25,27] We therefore restrict our attention and analysis to Hg-drop junctions.

Table 2. Values of β (See Eq 1) for Hg-Drop Junctions with SAMs of SC_n

N_C	junction	method^a	V^b (V)	β (Å⁻¹)	ref
9−20	Ag-SC$_n$S-Hg	AS-DEP	0.4	0.66	51
9−20	Ag-SC$_n$SH//Hg	AS-DEP	0.4	0.84	51
9−18	Hg-SC$_n$SH//Hg	n/a	0.4	0.85	52
10−18	Ag-SC$_n$//Hg	AS-DEP	0.4	0.82	51
16−24	Hg-SC$_n$//C$_n$S-Hg	n/a	0.4	0.82	52
24−32	Ag-SC$_n$//C₁₆S-Hg	AS-DEP	0.5	0.87	21
20−28	Ag-SC$_n$//C$_n$S-Hg	TS	0.5	0.57	TW^c
20−28	Ag-SC$_n$//C$_n$S-Hg	TS	0.5	0.64	TW^d
8−28	Hg-SC$_n$//C$_m$S-Hg	n/a	−1.5	0.71	54
18−24	Hg-SC$_n$//C$_n$S-Hg	n/a	1.5	1.0	49

^{a} The method used to form the (non-mercury) metal substrate, where AS-DEP and TS are described in the text. ^{b} The applied voltage at which J is recorded. ^{c} This value for β is calculated using the log-mean values of J measured in this work. ^{d} This value for β is calculated using the minimum values of J measured in this study (see the Results and Discussion section for more details.)
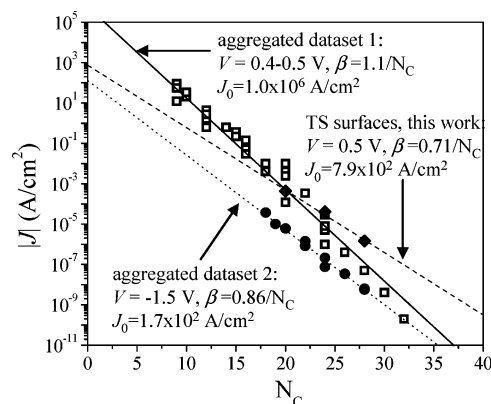

Figure 1. Log J for Hg-drop junctions incorporating SAMs of *n*-alkanethiolates vs the total number of carbons in the alkyl chain(s) between the electrodes in the junction (y-axis = log(column 5) of Table 1, and x-axis = column 1 of Table 1). The slope of the linear least-squares fit to these data is $\beta/2.3$ (where β is defined in eq 1). In the calculation of β, all points are weighted equally. Aggregated dataset 1 (◆, □) includes values of J measured at $V = 0.4$ or 0.5 V (the ◆ are data from this paper acquired using TS surfaces). For this dataset, $\beta = 1.1/N_C$ (0.85 Å⁻¹), and $J_0 = 1.0 \times 10^6$ A/cm². Aggregated dataset 2 (●) contains values of J measured at $V = −1.5$ V. For this dataset, $\beta = 0.86/N_C$ (0.69 Å⁻¹), and $J_0 = 1.7 \times 10^2$ A/cm².

Table 1 lists all reported current densities measured through self-assembled monolayers or bilayers of *n*-alkanethiolate or *n*-alkane-α,ω-dithiolate within MIM junctions comprising either one mercury electrode and one thin-film metal electrode, or two mercury electrodes. The entries in this table are grouped according to the total number of carbons (N_C) in the alkyl chain-(s) that separate the two electrodes. The final column lists the ratio of the maximum and minimum values of J measured for each group—as log(J_{max}/J_{min})—that is, the range of J across the set of reported measurements for analogous junctions. For example, the range of J across the largest set of analogous junctions—those with 24 carbons separating the two electrodes ($N_C = 24$)—is 1.6 orders of magnitude. The values of J collected at $V = −1.5$ V were not included in the calculation of log-(J_{max}/J_{min}). Table 2 lists β for all of the junctions in Table 1 for which this value is available.

Figure 1 is a plot of log J vs N_C (from the data in Table 1). A linear least-squares fit ($R^2 = 0.971$) to the largest dataset—that collected at $V = 0.4−0.5$ V—yields $\beta = 1.1/N_C$ (0.85 Å⁻¹). We disregard two features of the experiments that we cite when plotting all of the values of J in Table 1 against the common
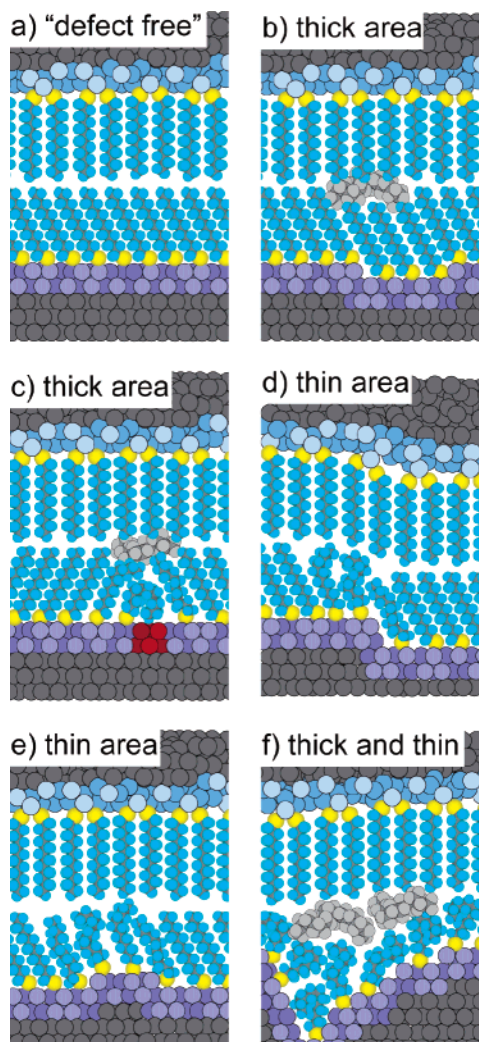
Figure 2. Schematic diagrams of several possible defects in SAMs of SC_{12} on silver (bottom electrode) and at the interface with a SAM of SC_{12} on mercury (top electrode): (a) a defect-free junction; (b) isolated (un-annealed) vacancies; (c) impurities in the silver film that cause local disorder in the SAM; (d) steps at the edge of annealed vacancy islands; (e) small, raised vacancy islands; and (f) defects at the grain boundaries of the silver supporting disordered SAMs. The molecules in between the SAMs are intercalated or trapped solvent (e.g., hexadecane) or solute (e.g., HSC_{12}) molecules.

axis N_C. (i) The value of d_0 for all of these junctions is not the same: some have two chemisorbed metal−molecule interfaces, and some have one chemisorbed and one physisorbed metal−molecule interface (i.e., a van der Waals contact between the hydrogen atom of the terminal methyl group of the thiolate molecule and the metal). While the value of β for a set of data taken using a single experimental setup does not depend on d_0, the value of β obtained from a set of data taken on multiple systems, such as that plotted in Figure 1, *does* depend on the relative values of d_0 of its component datasets. (ii) There are probably charge transport pathways (intermolecular pathways) that contribute to J that do not lie exclusively along the carbon backbone of one alkyl chain.[26] The alkyl chains within the bilayer junctions might also intercalate at the SAM//SAM interface. Intercalation of the thiolate molecules would probably result in charge transport pathways that do not incorporate all of the carbon atoms of both SAMs.

An Introduction to Defects in Ag-SAM//SAM-Hg Junctions. The SAM and the metal−molecule interface may include

several types of defects (Figure 2). In this work, we neglect possible defects in the SAM on mercury, since these SAMs are well-packed and lack the topographically induced defects present in SAMs on silver.[33−35,50,55] At the sites of some of these defects (for example, those pictured schematically in Figure 2b,c), randomly oriented solvent or solute molecules can be trapped between the SAM on silver and the SAM on mercury.[56] The "through-solvent" pathway for electron transport involves tunneling across more van der Waals interfaces than does the covalent pathway, and we expect J through these defects−or "thick areas"−to be lower than J through sites that lack defects (Figure 2a). At the sites of defects of the type represented in Figure 2d,e, the SAM on the mercury contacts an area of the SAM on the silver film that is disordered−a "thin area". We expect that J through these defects is higher than J through sites that are defect-free. Certain defects, like the metal grain boundary pictured in Figure 2f, contain both thick and thin areas; the current through thin areas dominates the current through these defects.

In this study, we observed a decrease of several orders of magnitude in the range of J and a large decrease in the percentage of junctions that shorted as a result of amalgamation of the mercury and silver electrodes upon switching from AS-DEP to TS silver substrates. We propose that (i) we can account for the large range of current densities and the poor electrical stability of the AS-DEP junctions relative to those of the TS junctions by considering a variety of defects that we will describe in detail (most notably, thin areas) and (ii) the types of defects that exist in Hg-drop junctions may also be present in other types of molecular junctions, but the electrical characteristics that result from a certain set of defects may vary from system to system.

Nomenclature. We denote SAMs of *n*-alkanethiolate as SC_n or C_nS, where the subscript "*n*" refers to the number of carbons in the alkyl chain ($SC_n \equiv S(CH_2)_{n-1}CH_3$). As previously,[18,20,44] "Ag-SC_n" is a silver thin-film electrode supporting a SAM of SC_n, and "C_nS-Hg" is a mercury electrode supporting a SAM of SC_n. The symbol "-" indicates the presence of a chemical bond, and "//" indicates the presence of a van der Waals interface in a junction.

Experimental Section

Fabrication of Electrodes. To form the AS-DEP substrates, we deposited an adhesion layer of titanium (2 nm) and then a layer of silver (40 nm) onto a clean, dry silicon wafer supporting its native oxide layer ("Si/SiO₂") using an electron-beam (e-beam) evaporator. When we were not able to form the SAM and characterize the MIM junctions on the same day that we evaporated the silver films, the films were stored in a vacuum desiccator (at ∼50 mTorr) for no longer than 3 days before use.[12,57]

(54) Slowinski, K.; Fong, H. K. Y.; Majda, M. *J. Am. Chem. Soc.* **1999**, *121*, 7257.
(55) When SAMs on mercury drops are used as conformal electrodes, they are subject to mechanical deformation. The effect of these stresses on the quality of the SAM has not been characterized. We hypothesize that it will be less for SC_{12} (which is probably relatively liquid-like, and thus laterally mobile) than with longer chains (e.g., SC_{18}, which are more crystalline and probably more brittle and subject to fracture into plates, rather than simple lateral spreading).
(56) The surface tension of mercury (480 dyn/cm) is high [Nicholas, M. E.; Soyner, P. A.; Tessen, B. M.; Obson, M. E. *J. Phys. Chem.* **1961**, *65*, 1373], even when lowered by the presence of the SC_{12} (effectively a surfactant for the metal). The mercury electrode (supporting a SAM of SC_{12}, heretofore referred to as the Hg-SC_{12} electrode) will, therefore, conform to some changes in the topography of the silver film but will not conform to others.
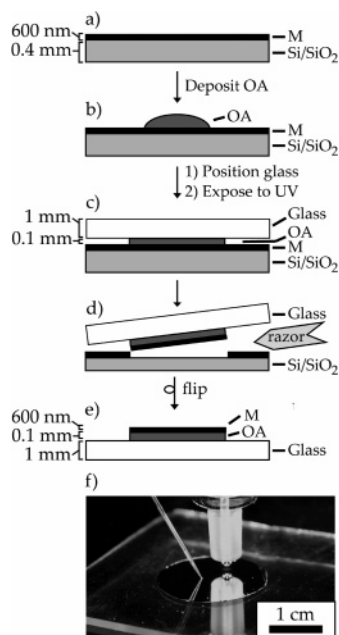(57) Ulman, A. *Chem. Rev.* **1996**, *96*, 1533.

Figure 3. Schematic diagram of template stripping. (a) We deposit a metal onto a Si/SiO$_2$ template and (b) put a drop of optical adhesive (OA) onto the metal film. (c) The OA adheres a glass slide to the surface of the metal. (d) We use a razor to manually cleave the glass/OA/metal composite and separate it from the silicon template. (e) The smooth surface of the metal that was at the silicon interface is exposed. (f) Photograph of a template-stripped Ag surface on a glass mechanical support and contacted with a gold needle. Above the surface hovers a drop of mercury suspended from a syringe (see Figure 4 and its caption for a schematic and description of the Hg-drop junction).

The general procedure for template-stripping[58] is to deposit a metal onto an atomically flat template (mica, Si/SiO$_2$, float glass; we used Si/SiO$_2$ in this work), coat the metal with a backing (nickel[9], epoxy[7]), and peel the metal/backing composite from the substrate to expose the surface of the metal that had been at the metal/template interface. In our procedure (Figure 3), we used a mechanical backing consisting of glass that was glued to the metal film with optical adhesive (OA, Norland, no.61).[59] Using an e-beam evaporator, we deposited a 600-nm-thick layer of silver onto a Si/SiO$_2$ template and applied a drop (~0.1 mL) of OA to the silver film. We rinsed a glass slide (1.2 mm thick, cut into 1-cm^2 pieces) with ethanol and acetone, dried it under a stream of N$_2$, exposed it for 5 min to plasma oxidation, and immediately (within 1 min) placed it on top of the OA. Under the weight of the glass slide, the OA spread over nearly the entire area of the silver film that was covered by the glass slide (without any additional pressure). A 0.1-mL drop of OA covered an area of ~1 cm^2 evenly with a thickness of ~0.1 mm. Exposure to ultraviolet light (long-wave mercury lamp, 100 W) for 1 h through the glass cured the OA and bound the glass to the silver film. We needed a longer irradiation time than that necessary to achieve mechanical hardening of the polymer (15–20 min) in order to minimize diffusion of un-cross-linked material from the backing to the surface of the silver through cracks or pinholes. We cleaved the glass/OA/silver composite from the Si/SiO$_2$ template by running a razor blade around the edge of the interface between the OA and the silver and then applying gentle pressure to the side of the glass mechanical support in a direction parallel to the plane of the Si/SiO$_2$. This procedure exposed the silver surface that had been in contact with the atomically smooth Si/SiO$_2$ template. The e-beam evaporation did not occur under ultra-high-vacuum conditions—rather, it occurred at pressures only as low as ~10^{-6} Torr; therefore, some amount of oxidation of the silver occurred during this process. Uncleaved

(58) Hegner, M.; Wagner, P.; Semenza, G. *Surf. Sci.* **1993**, *291*, 39.
(59) Weiss, E. A.; Kaufman, G. K.; Kriebel, J. K.; Li, Z.; Schaleck, R.; Whitesides, G. M., submitted to *Langmuir*.
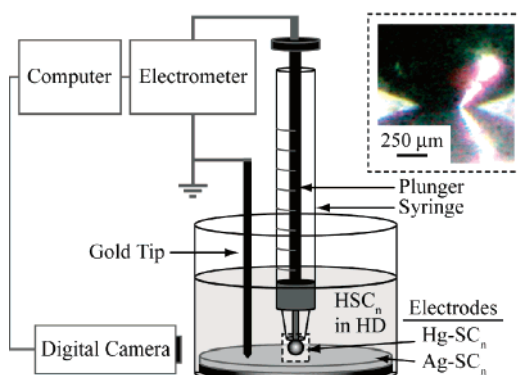
Figure 4. Schematic drawing of the apparatus used to measure the tunneling current through Hg-drop junctions. The electrometer (controlled by a program written in LabVIEW) applies voltage to the mercury electrode and holds the silver electrode at ground. The electrical circuit is as follows: (i) the electrometer connects to the metallic interior of the plunger; (ii) a tungsten wire extends from the metallic interior, through the Teflon seal of the plunger, and into the mercury reservoir held by the syringe; (iii) the mercury supports a SAM that is in van der Waals contact with the SAM on the Ag electrode (Ag-SC$_n$//C$_n$S-Hg); and (iv) the Ag electrode connects to ground via a gold tip in mechanical contact with the surface. The area of the junction was imaged by a digital camera from the side—the inset shows a photographic image of the side of a TS Ag-SC$_{12}$//C$_{12}$S-Hg junction.

composites (i.e., those in which the silver remained on the silicon substrate in a Si/SiO$_2$/Ag/OA/glass "sandwich structure") could, however, be stored for at least 1 month without a significant increase in the amount of oxide on the TS surface (Supporting Information). Once the composite was cleaved, we immersed the TS surfaces in a solution containing an alkanethiol within 15 s to form SAMs (as described in the next section). The combination of OA and a Si/SiO$_2$ template reliably produced smooth surfaces in nearly 100% yield.[59]

Formation of the SAMs of *n*-Alkanethiolate on Ag. The SAMs of SC$_n$ formed for at least 8 h on the TS or AS-DEP silver surfaces at room temperature in 1 mM ethanolic solutions of decanethiol (HSC$_{10}$), dodecanethiol (HSC$_{12}$), or tetradecanethiol (HSC$_{14}$) (see Supporting Information for more details).

The Hg-Drop Junction. The Hg-drop junction in this work consists of a mercury electrode[18] that supports a SAM of SC$_n$ and contacts a SAM of SC$_n$ supported by a silver electrode (Figure 4), where n = 10, 12, 14. We formed these symmetric bilayer junctions by extruding a new drop of Hg from the syringe (inner diameter = 1 mm) under a solution of HS(CH$_2$)$_{n-1}$CH$_3$ (1 mM) in hexadecane to form a new SAM of SC$_n$ on this Hg drop (see Supporting Information) and bringing the Hg-SC$_n$ electrode into contact with an unused area on the Ag-SC$_n$ electrode. Immersing the junction in a liquid medium (in this case, the solution in which the SAM on the Hg drop was formed) during the J–V measurements helped to prevent amalgamation of the Hg-SC$_n$ and Ag-SC$_n$ electrodes: when we attempted to carry out measurements in air, with no stabilizing liquid, amalgamation of the electrodes occurred consistently on the first scan.

An electrometer was used to apply a voltage (V) across the junction (immersed in the solution of thiol in hexadecane) by holding the silver electrode at ground and changing the voltage at the mercury electrode (Figure S1, Supporting Information). The electrometer measured the values of the current (after a 2 s delay once the bias was applied) at each applied voltage (0 V → +0.5 V → −0.5 V → 0 V, in 0.05 V steps). A home-made program in LabVIEW recorded the data. The choice of this range of potentials is based on three considerations: (i) ±0.5 V extends well beyond the "low-bias" regime, where current depends only linearly on voltage; (ii) this range is often used for electrical measurements on MIM junctions that incorporate alkane-thiolates, so we can easily compare our data with those of other groups; and (iii) these minimum and maximum voltages are below the voltage

a) AS-DEP

b) TS
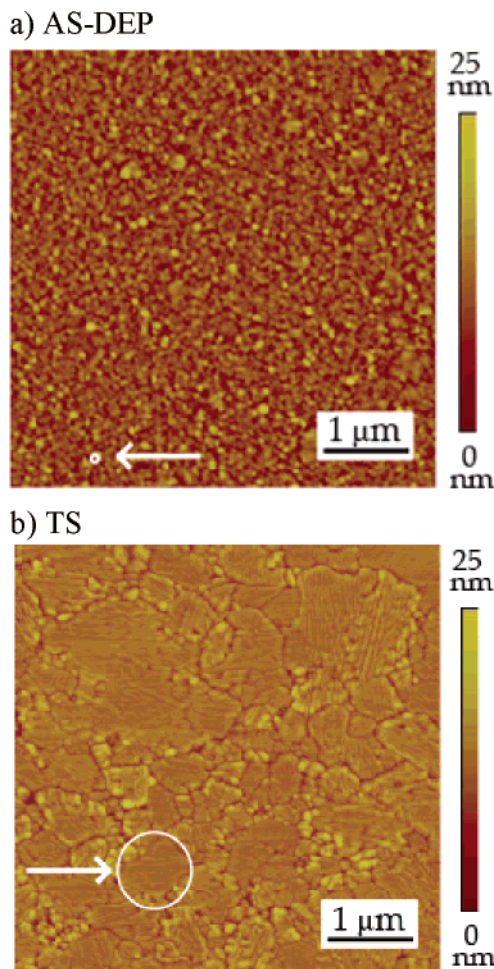
Figure 5. Contact-mode AFM images of the topography of the (a) AS-DEP silver film and (b) TS silver film. The root-mean-square roughnesses of a 25 μm^2 area of the silver films are 5.1 ± 0.4 nm for AS-DEP and 1.2 ± 0.1 nm for TS. The white circles indicate the approximate size of the largest grains in each film and have diameters of (a) AS-DEP, 80 nm, and (b) TS, 1 μm.

at which the thiolate desorbs from the surface (−1.0 to −1.4 V on Ag).[60]

A camera (Edmund Industrial Optics) captured a magnified image of the junction from the side. An NTSC capture card digitized the image, and we measured the diameter of the junction on the computer screen. The areas of our junctions ranged from ~3.1 × 10^{-4} to ~2.8 × 10^{-3} cm^2.

Results and Discussion

Comparison of the Topography of TS and AS-DEP Silver Surfaces: AFM. We used AFM in contact mode to determine the topography of the bare AS-DEP and TS silver films (Figure 5). The root-mean-square roughness was 5.1 ± 0.4 nm for the AS-DEP film and 1.2 ± 0.1 nm for the TS film (both over an area of 25 μm^2). The latter roughness is one of the lowest reported for silver (Diebel and co-workers reported a root-mean-square roughness of ~0.3 nm over an area of <1 μm^2, obtained using a procedure similar to ours).[61] The maximum grain size was ~1 μm^2 for the TS surface and ~0.0064 μm^2 for the AS-DEP surface. The overall smoothness of, and the presence of

(60) Azzaroni, O.; Vela, M. E.; Andreasen, G.; Carro, P.; Salvarezza, R. C. *J. Phys. Chem. B* **2002**, *106*, 12267.
(61) Diebel, J.; Lowe, H.; Samori, P.; Rabe, J. P. *J. Appl. Phys. A* **2001**, *73*, 273.
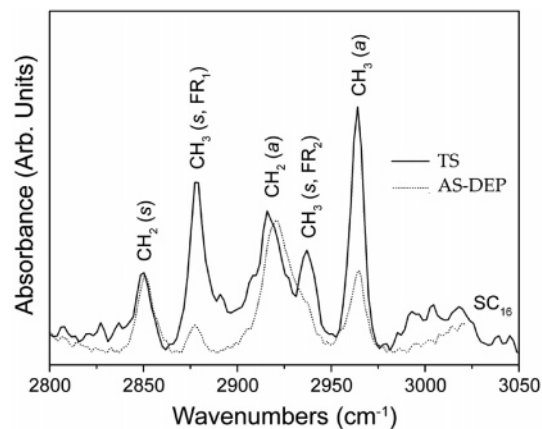
Figure 6. Plots of the C−H stretching region of the RAIR spectra for the SAMs of SC$_{16}$ on TS silver and on AS-DEP silver. The spectra were smoothed by five-point adjacent averaging. The symmetric and asymmetric methylene stretching peaks are at higher energies for SAMs on AS-DEP silver than for SAMs on TS silver, an indication that the SAMs on AS-DEP silver are less ordered than those on TS silver.

large grains on, the TS surface correspond to a reduction in the density of defects (grain boundaries, step edges, etc.) on the surface from that on the AS-DEP surface.

Dependence of Intermolecular Packing on Roughness and Grain Size: Reflectance−Absorbance Infrared (RAIR) Spectra. We examined the C−H stretching region of the IR spectra of SAMs of SC$_{16}$ on AS-DEP and TS surfaces of silver (Figure 6) to determine the effect of surface topography on intermolecular order. We chose SC$_{16}$—despite the fact that the values of J that we measured for the Ag-SC$_{16}$//C$_{16}$S-Hg bilayer junctions were below the detection limit for this particular experimental setup—because it is highly ordered[3,12] (the crystallinity of SAMs of SC$_n$ increases with increasing chain length), and thus it is a good system with which to study substrate-induced disorder in the SAMs.

The frequencies of the symmetric and asymmetric methylene stretching modes are especially sensitive to intermolecular packing (the average energies of these vibrations increase with increasing intermolecular disorder).[62,63] As reported by us[59] and others,[63] a comparison of the frequencies of these vibrations in molecules comprising SAMs on TS and AS-DEP silver with those of the same molecules in the bulk crystalline phase (ν_s-(CH$_2$) = 2848−2851 cm^{-1} and ν_a(CH$_2$) = 2918 cm^{-1}) reveals that (i) the SAMs of SC$_{16}$ that we formed (on all surfaces) were more like a 2D solid than like a 2D liquid; (ii) peaks for the symmetric and asymmetric methylene stretches were at higher energies (by ~4 cm^{-1} for SAMs of SC$_{16}$) in the spectra of SAMs on AS-DEP surfaces than in the spectra of SAMs on TS surfaces; and (iii) the asymmetric methyl stretch, ν_a(CH$_3$), and the component of the symmetric methyl stretch at ~2877 cm^{-1}, ν_s(CH$_3$, FR$_2$),[64−66] are markedly more intense (relative to the ν_s(CH$_2$) band) in the spectrum of the SAM on TS silver than in the spectrum of the SAM on AS-DEP silver (and, thus, the ratio

(62) Porter, M. D.; Bright, T. B.; Allara, D. L.; Chidsey, C. E. D. *J. Am. Chem. Soc.* **1987**, *109*, 3559.
(63) Blackstock, J. J.; Li, Z.; Stewart, D. R.; Isaacson, K.; Kwok, D. Y.; Freeman, M. R.; Green, J.-B., unpublished work.
(64) The symmetric methyl stretch is split into two components, at 2937 and 2877 cm^{-1}, due to Fermi resonance interactions with a low-frequency asymmetric methyl deformation mode.
(65) Dubois, L. H.; Nuzzo, R. G. *Annu. Rev. Phys. Chem.* **1992**, *43*, 437.
(66) Zhang, M.; Anderson, M. R. *Langmuir* **1994**, *10*, 2807.

$\nu_s(CH_2):\nu_s(CH_3)$ is smaller for the SAM on TS silver than for the SAM on AS-DEP silver). A higher ratio of the intensity of the $\nu_s(CH_2)$ band to the intensity of the $\nu_s(CH_3)$ bands indicates a higher average tilt angle of the molecules on the surface, possibly as a result of lower molecular density and increased disorder in the SAM.[63] This observation, coupled with the shift to lower frequency of the asymmetric and symmetric methylene stretches in the spectrum of the SAM on TS silver, implies qualitatively that the SAM on TS silver is more ordered than the SAM on AS-DEP silver.[66,67] It is not practical to try to quantify the order in these samples without a level of spectroscopic analysis that is beyond the scope of this paper.

Description of Defects in Films of Ag−SC$_n$. There are several types of defects that contribute either to failure of a junction or to artificially high or low current density through a junction. The set of defects within SAMs on Ag fit into three main categories: (i) metal filaments, which lead to amalgamation and failure for Hg-drop junctions (hence the exclusion of filaments from Figure 2) but result in artificially high J in junctions with two solid metal electrodes; (ii) "thick areas", defined as those defects in which solvent or solute molecules separate the SAM on silver and the SAM on mercury; and (iii) "thin areas", defined as those defects in which the SAM on mercury contacts an area of the SAM on silver that is disordered, and in which the electrode-to-electrode distance is less than in the crystalline ordered regimes of the SAM. We discuss each of these classes in turn in the following.

(a) Filaments. Migration of metal atoms from the surface of one electrode to the second electrode results in a highly electrically conductive pathway between the electrodes.[68] We believe that it is reasonable to assume that the magnitude of the current through a metal filament is similar to that through a metal nanowire. Measured and calculated values for current (I) through gold and silver nanowires at an applied voltage of ~0.5 V are consistently on the order of 0.1 mA.[69−73] For a hypothetical junction with a current density of 10^{-5} A/cm^2 and an area of 0.1 mm^2 ($I = 10$ nA; values similar to those for the junction Ag-SC$_{12}$//C$_{12}$S-Hg), the current through just one filament ($I = 0.1$ mA) would account for >99.9% of the total current through the junction and would be independent of the molecular structure of the SAM. It is likely that filaments are responsible only for the behavior that leads to values of J that are 10^2-10^4 greater than the average J−values that we observe immediately before amalgamation occurs—or that the junction amalgamates before we record the current through the filament.

We thus believe that filaments do not contribute significantly to the distribution of current densities that we measured.

(b) Thin-Area Defects. Step edges (Figure 2d), raised vacancy islands (Figure 2e), and grain boundaries (Figure 2f) in the silver surface probably result in "thin areas" of the SAM, where the molecules are not *trans*-extended and the Hg-SC$_n$ electrode contacts a disordered region of the SAM on the silver film; this type of defect results in a reduced distance between the electrodes. In thin-area defects, competing factors influence the magnitude of the tunneling current: the tunneling pathway—whether through-space or through-bond—will plausibly be shorter for a thin region, but tunneling is more probable in *trans*-extended through-bond pathways than through intermolecular or *gauche* pathways. We assume that, on average, tunneling currents will be higher in these regions. Raised vacancy islands, which arise when metal atoms form small clusters on the surface that are one atomic step above the surrounding atoms rather than migrate to step edges, occur more frequently on silver than on gold. The molecules on the edges of raised vacancy islands are not stabilized by neighboring molecules and become disordered (or perhaps deformed) under the pressure of the mercury electrode.[12]

To explore theoretically the potential consequences of thin-area defects, we calculated the total current that passes through a heterogeneous SAM whose nominal thickness d_i is 2.75 nm (approximately the thickness of an SC$_{12}$//C$_{12}$S bilayer) as a function of the nominal thickness and fraction of the surface area covered by thin, defective regions (Figure 7a). In this model, the current density decays exponentially with distance, so that total $J = (x)J_0 e^{-\beta d} + (1 - x)J_i$, where x is the fraction of the total area of the junction that is covered by "thin area", $\beta = 0.6$ Å^{-1}, $J_0 = 2.0 \times 10^2$ A/cm^2, the electron follows a path of length d between the two electrodes, and $J_i = 1.4 \times 10^{-5}$ A/cm^2 is the total J through a junction composed of a defect-free SAM. Figure 7b shows the same data in terms of the percentage of the total current density that passes through the thin regions, where %J through "thin area" = $(x)J_0 e^{-\beta d}/$ total J. The key conclusion—obvious but important—from these plots is that current through thin areas can completely dominate the total current measured through the junction. Thus, for example, in a monolayer that is nominally 2.75 nm thick, if these defects are 1.5 nm thick, a 2% density of defects would carry >85% of the current (assuming that current still proceeds purely by tunneling). In the following, we will present evidence that suggests that thin-area defects are almost entirely responsible for the variance in J measured through the TS junctions.

(c) Thick-Area Defects. Within "thick-area defects", randomly oriented hexadecane (and, possibly, thiol) molecules are trapped in gaps at the SAM//SAM van der Waals interface (Figure 2b,c). These types of defects, in principle, decrease J relative to that through a defect (solvent)-free junction, although we may not be able to detect such an effect with the level of sensitivity of our measurement. Unlike thin-area defects, unless the junction is dominated by thick-area defects—for example, a layer of solvent covers the entire interface between the SAM on Hg and the SAM on Ag—the *percentage* of the total current through a junction that can be attributed to these defects is small because the magnitude of the current that passes through this defect is small (and the contribution of this current to the total current is the product of its magnitude with the percentage of

(67) The IR spectra of the SAMs of SC$_{16}$ formed on mechanically template-stripped silver (i.e., silver surfaces that are manually cleaved from the template before being submerged in the solution of thiol, as is done in this work) indicate that these SAMs are not as consistently well-ordered as those formed on chemically template-stripped silver. Chemical template-stripping involves submerging the entire "sandwich structure" (glass/OA/silver/SiO$_2$) in a thiol solution and allowing the silver to cleave from the template as the SAM forms [Weiss, E. A.; Kaufman, G. K.; Kriebel, J. K.; Li, Z.; Schaleck, R.; Whitesides, G. M., submitted to *Langmuir*].
(68) Haynie, B. C.; Walker, A. V.; Tighe, T. B.; Allara, D. L.; Winograd, N. *Appl. Surf. Sci.* **2003**, *433*, 203.
(69) Calleja, M.; Tello, M.; Anguita, J.; Garcia, F.; Garcia, R. *Appl. Phys. Lett.* **2001**, *79*, 2471.
(70) Mehrez, H.; Wlasenko, A.; Larade, B.; Taylor, J.; Grutter, P.; Guo, H. *Phys. Rev. B* **2002**, *65*.
(71) Park, H.; Lim, A. K. L.; Alivisatos, A. P.; Park, J.; McEuen, P. L. *Appl. Phys. Lett.* **1999**, *75*, 301.
(72) Park, S. H.; Barish, R.; Li, H.; Reif, J. H.; Finkelstein, G.; Yan, H.; LaBean, T. H. *Nano Lett.* **2005**, *5*, 693.
(73) Mozos, J. L.; Ordejon, P.; Brandbyge, M.; Taylor, J.; Stokbro, K. *Nanotechnology* **2002**, *13*, 346.
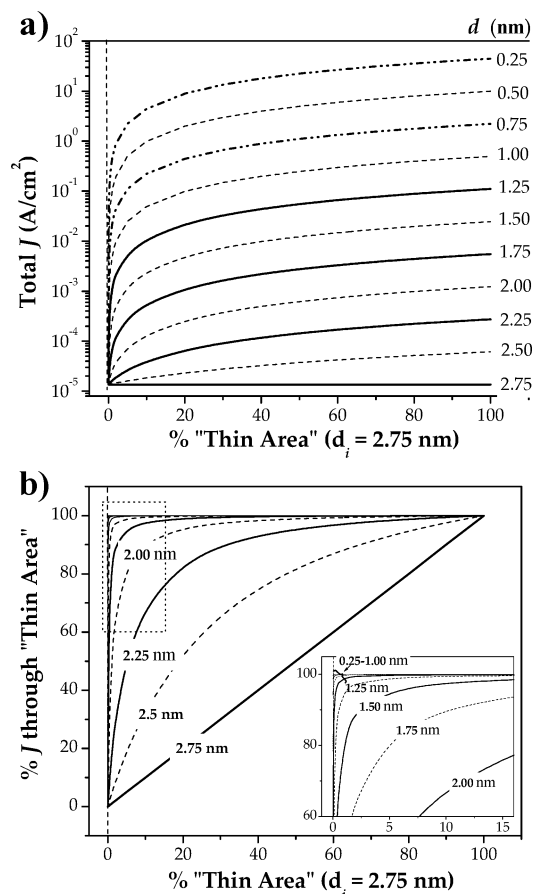
Figure 7. (a) Plot of the predicted total current density (Total *J*) through a hypothetical insulating layer with thickness $d_i = 2.75$ nm versus of the percentage of junction area covered by "thin area" ($d < d_i$) for % Thin Area = 0%, 0.1%, 1%, 10%, 20%, ..., 90%, 100%. Total $J = (x)J_0 \, e^{-\beta d} + (1 - x)J_i$, where *x* is the fraction of the total area of the junction that is "thin area", $J_0 = 2.0 \times 10^2$ A/cm², $d_0 = 0$, $\beta = 0.6$ Å⁻¹, and J_i = the current density through a defect-free insulating layer = 1.4×10^{-5} A/cm². We chose values of *d* that correspond to shortening the insulating layer by two, four, six, etc. methylene groups within a *trans*-extended alkyl chain (where the distance between adjacent carbons along the molecular axis is 0.125 nm). (b) Plot of the percentage of current density through "thin area" in the SAM as a function of the percentage of junction area that is covered by these defects, where %*J* through "thin area" = $(x)J_0 \, e^{-\beta d}/$Total *J*. For reference, in both (a) and (b), we plotted the limiting case $d = d_i = 2.75$ nm. We inserted a dotted line at $x = 0$ in both plots to guide the eye.

the junction area that is covered by defects). The contribution of thick-area defects gets *smaller* as the defect gets "thicker"—that is, it deviates more from the nominal thickness of the SAM. It is, nonetheless, instructive to discuss the origins of such defects in films of alkanethiolate on silver.

Solvent molecules can become trapped within a gap at the SAM//SAM van der Waals interface when a molecule "kinks"—that is, bends over within the SAM and curls away from the interface with the top contact. If one chain bends, another chain will bend on top of it, and packing of the terminal ends of the chains of the few surrounding molecules will be more disordered than that of fully *trans*-extended chains. This disorder is evident in the IR spectra of the TS and AS-DEP SAMs (Figure 6). Aside from the presence of grain boundaries or step edges in the metal film, molecules kink for (at least) three reasons. (i) Impurities in solvents and reagents deposit on the metal surface during SAM formation and cause irregularities in the metal lattice (the red spots in Figure 2c).[3,74,75] These defects are extrinsic, and

careful control of experimental methods can minimize them.[76] (ii) Single-molecule-sized holes in the SAM prevent the alkyl chains from packing and allow surrounding molecules to kink. (iii) The alkyl chains of a molecule have multiple *gauche* defects that result in a kinked conformation. The formation of thermally driven populations of *gauche* conformers is intrinsic: that is, due to the dynamics of the organic component of the SAM and to entropy. These defects are thus inevitable, even in highly crystalline arrays.

Solvent molecules may also collect at the SAM//SAM interface at the site of an isolated or un-annealed vacancy island in the silver film. Vacancy islands form when individual silver atoms dissociate from the plane of the silver surface upon formation of the thiolate bond and migrate to form raised islands.[3,77,78] The reorganization process leaves vacancies of one or a few metal atoms that are one atomic step (~0.5 nm for silver) below the surface (Figure 2b); heat induces further reorganization into larger-area annealed vacancy islands.[77,78]

The Role of Defects in the Electrical Characteristics of the Junctions Ag-SC*n*//SC*n*-Hg. (a) Typical Behavior of the Junctions under Applied Voltage: Solvent Expulsion and Amalgamation. Figure 8a shows a typical set of |*J*|−*V* curves for a TS junction (in this case, the junction Ag-SC₁₀//C₁₀S-Hg): the first full, or nearly full, voltage sweep yielded current densities a factor of ~10⁴ less than that for subsequent sweeps, during which the current density increased slightly (usually by only a factor of 5) before stabilizing. Before voltage is applied, solvent molecules can collect at the interface between the SAMs or be trapped at the sites of defects. The randomly oriented solvent molecules present a set of van der Waals interfaces that are highly resistive to tunneling and, we assume, lower the current density through the junction. As voltage is applied to the junction, charge builds up at the surface of each electrode. The electrostatic pressure exerted by the surfaces of the junction increases; this pressure causes the mercury drop to deform and expels solvent from the junction. We suspect that the transition from an initial, low-current trace to a set of reproducible, higher-current traces measured for most of the TS samples reflected expulsion of solvent by this mechanism, a phenomenon also observed by Majda.[54] Once the SAM on Hg and the SAM on Ag were in contact, repeated cycling of the voltage deformed the Hg drop and caused the junction to grow in area. Inspection of the junction after the measurements revealed that the junction area increased consistently by an amount, usually a factor of 1.2−2.0, that depended on the number of cycles the junction endured. The error in estimating the size of the junction introduces an error in *J*. We will discuss these errors in detail later.

Figure 8b shows the typical behavior of *J* through a junction that amalgamated. Directly preceding amalgamation, the current

(74) Hoogvliet, J. C.; van Bennekom, W. P. *Electrochim. Acta* **2001**, *47*, 599.
(75) Hieber, H. *Thin Solid Films* **1976**, *37*, 335.
(76) In general, the assembly of a SAM involves a dynamic exchange between adsorbates on the surface and their precursors in free solution [Love, J. C.; Estroff, L. A.; Kriebel, J. K.; Nuzzo, R. G.; Whitesides, G. M. *Chem. Rev.* **2005**, *105*, 1103]. The composition of a SAM reflects (i) the concentration of the adsorbate species present in the solution, (ii) the strength of the intermolecular interactions among adsorbate species in solution and in the SAM, (iii) the strength of the bond between the adsorbate molecule and the metal surface, and (iv) the presence of kinetically trapped defects and disorder in the array reflecting inevitable entropic disorder.
(77) Bucher, J.-P.; Santesson, L.; Kern, K. *Langmuir* **1994**, *10*, 979.
(78) Dhirani, A.; Hines, M. A.; Fisher, A. J.; Ismail, O.; Guyot-Sionnest, P. *Langmuir* **1995**, *11*, 2609.
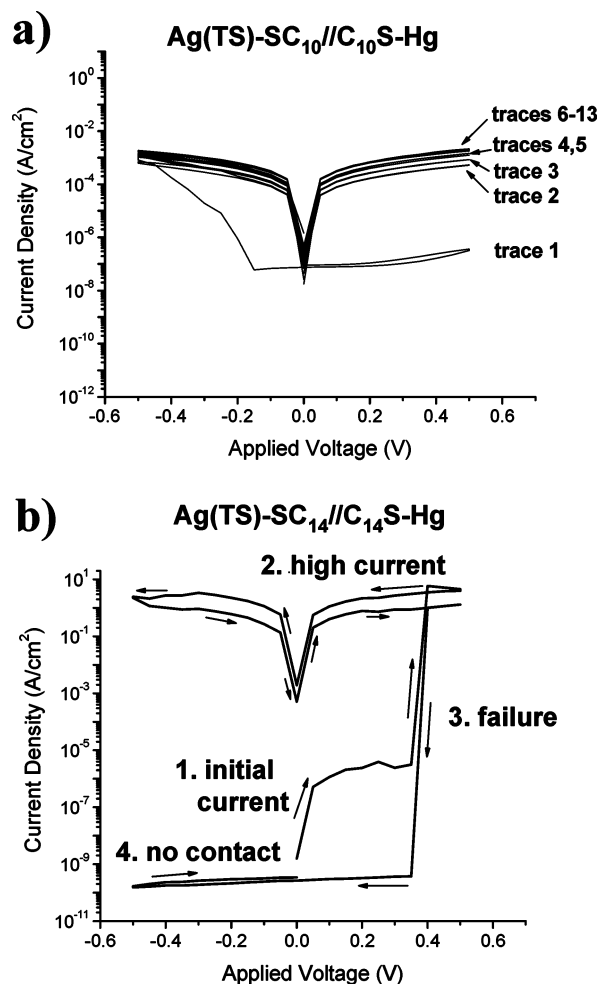
a)

Ag(TS)-SC$_{10}$//C$_{10}$S-Hg

traces 6-13
traces 4,5
trace 3
trace 2

trace 1

b)

Ag(TS)-SC$_{14}$//C$_{14}$S-Hg

2. high current

3. failure

1. initial current

4. no contact

Figure 8. (a) Set of $|J|-V$ curves for the TS junction Ag-SC$_{10}$//C$_{10}$S-Hg. The first full or nearly full voltage sweep yielded current densities $\sim10^4$ A/cm^2 less than those obtained for subsequent sweeps, which yielded currents that increased slightly (usually by only half an order of magnitude) before stabilizing. This behavior is representative of that of stable TS junctions Ag-SC$_n$//C$_n$S-Hg, where $n = 10$, 12, and 14. (b) Typical $|J|-V$ curve for a junction that amalgamated. Directly preceding amalgamation, the current jumped by several orders of magnitude from its initial value. Amalgamation resulted in a loss of electrical continuity in the circuit and current that was indistinguishable from that through an open circuit ("no contact" current).

jumped by several orders of magnitude from its initial value as the mercury penetrated the SAM through a defect (probably a thin area or pinhole). During amalgamation, the mercury drop at the tip of the syringe spread onto the surface of the silver electrode and lost contact with the mercury reservoir in the syringe. This process broke the mercury thread within the syringe and resulted in a loss of electrical continuity in the circuit (an "open circuit"). Table 3 gives the percentage of junctions (both TS and AS-DEP) that amalgamated during trace 1 (no full traces were completed), traces 1−3 (two or fewer traces were completed), and traces 1−5 (four or fewer traces were completed). This table incorporates data from two surfaces bearing SAMs formed on separate days, in separate solutions of thiol. Only the junctions for which either five traces were attempted or the junction amalgamated before five traces were completed were included in the statistics in Table 3. (One hundred percent of the AS-DEP Ag-SC$_{10}$//C$_{10}$S-Hg junctions failed before we completed five traces.) We intentionally stopped data collection after fewer than five traces for some junctions.

Table 3. Summary of the Failure Rate of the Junctions Ag-SC$_n$//C$_n$S-Hg with AS-DEP and TS Ag Surfaces

			% of junctions that failed during the specified trace(s)					
			1[b]		1–3		1–5	
	junctions[a]							
	TS	AS-DEP	TS	AS-DEP	TS	AS-DEP	TS	AS-DEP
SC$_{10}$	10	9	0	33	0	67	10	100
SC$_{12}$	13	9	0	0	0	11	15	33
SC$_{14}$	13	9	0	0	23	33	31	67
total	39	32	0	11	8	37	19	67

^{a} Total number of junctions—using two separate AS-DEP or TS surfaces—that either (i) survived five or more traces or (ii) amalgamated before five traces were completed. (With some junctions, fewer than five traces were attempted, and the junction did not amalgamate; the data from these junctions are included in Figures 9−11, but are omitted from this table.) ^{b} A trace is a scan of J vs V, where $V = 0$ V → 0.5 V → −0.5 V → 0 V.

Values of J from these junctions are included in Figures 9−11, but these junctions are not included in this table.

The AS-DEP junctions failed, on average, 4.6 times more often during traces 1−3, and 3.5 times more often during traces 1−5, than did TS junctions. In addition, we can summarize Table 3 as follows. (i) The AS-DEP Ag-SC$_{10}$//C$_{10}$S-Hg junctions were most susceptible to amalgamation. Three of those junctions failed during the first trace, and all failed eventually (after four or fewer traces). (ii) The AS-DEP Ag-SC$_{12}$//C$_{12}$S-Hg junctions were more stable than the AS-DEP Ag-SC$_{10}$//C$_{10}$S-Hg junctions. (iii) The AS-DEP Ag-SC$_{14}$//C$_{14}$S-Hg junctions amalgamated more often once one trace had been completed than the AS-DEP Ag-SC$_{12}$//C$_{12}$S-Hg junctions. (iv) The stability of TS junctions followed the trend Ag-SC$_{14}$//C$_{14}$S-Hg < Ag-SC$_{12}$//C$_{12}$S-Hg < Ag-SC$_{10}$//C$_{10}$S-Hg.

We can explain these results by noting that the increasing degree of crystallinity in the SAMs as the alkyl chains lengthen from $n = 10$ to $n = 14$ has two competing effects on the stability of the junctions. (i) As the alkyl chains in the SAMs get longer, the molecules depend less on the lattice of the underlying metal to form a well-ordered monolayer, because interchain van der Waals interactions increasingly provide a driving force for the ordering of the SAM. Tightly packed monolayers cover the surface of the Ag more completely—and, therefore, mitigate the degree to which defects *in the underlying metal substrate* translate into defects in the SAM—than do disordered mono-layers. (ii) At a certain length of the alkyl chain, the SAM becomes crystalline enough such that defects characteristic of crystalline materials (well-defined grain boundaries or cracks) form. These *intrinsic* defects (not resulting from defects in the underlying silver substrate) can initiate amalgamation. Mono-layers of SC$_{14}$ are the most crystalline of those we studied; these SAMs thus provide better coverage of the Ag surfaces—but also have a higher density of the aforementioned intrinsic defects—than do SAMs of either SC$_{10}$ or SC$_{12}$. From the data in Table 3, it appears that both of these factors are important on the rough AS-DEP substrates (where defects in the Ag largely determine the type and frequency of defects in the SAM, and, hence, the stability of the junction), while the latter effect dominates on the ultraflat, TS Ag substrates (where defects in the lattice of the SAM probably dominate the overall density of defects and, hence, determine the stability of the junction).

(b) The Magnitude, Distribution, and Distance Dependence of J. Figure 9 (left column) shows all of the $|J|-V$ curves
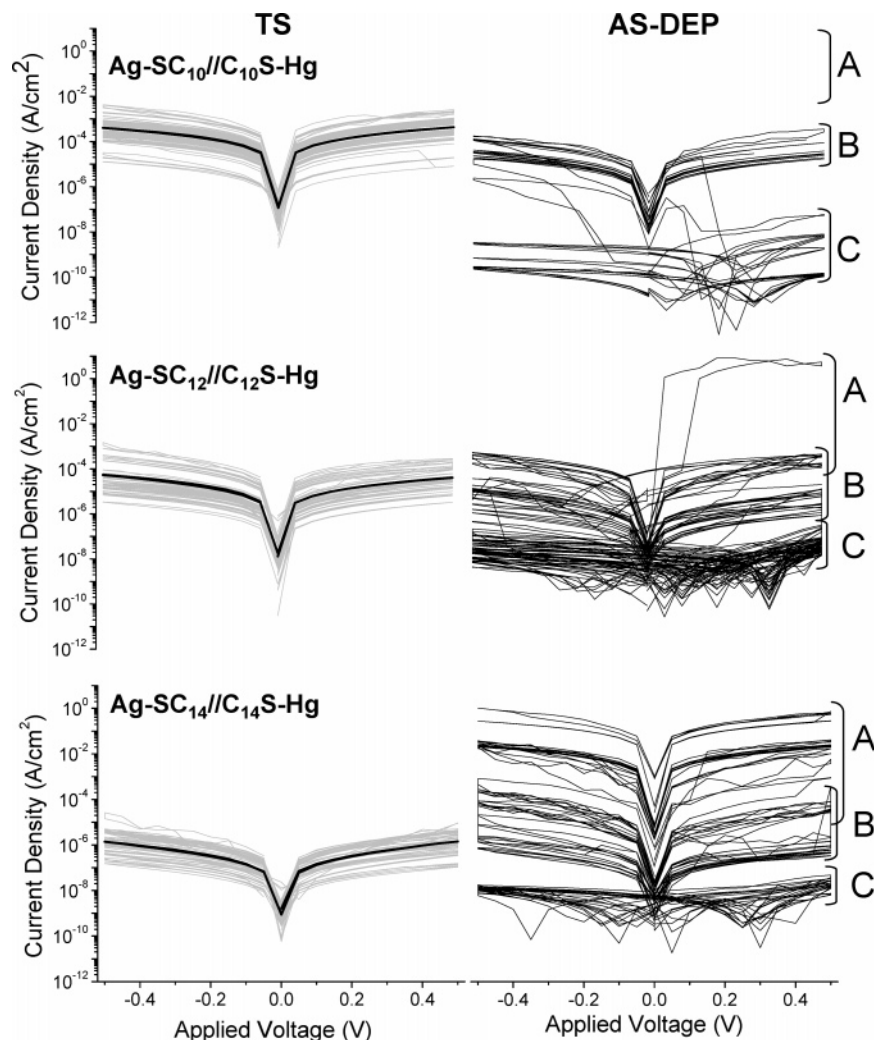
Figure 9. (Left) Plots of the average $|J|-V$ curves (log-mean, bold black lines) and all $|J|-V$ curves (light gray lines) measured on the TS junctions Ag-SC$_n$//C$_n$S-Hg ($n = 10, 12, 14$), except for the initial traces that had a current density several orders of magnitude below the remaining traces, and traces directly preceding and following amalgamation. (Right) The same set of traces for the corresponding junction using AS-DEP silver. (No averages were calculated for these data.) The designations "A", "B", and "C" are explained in the text.

(light gray lines) measured on the TS junctions Ag-SC$_n$//C$_n$S-Hg ($n = 10, 12, 14$) except for (i) initial traces that had a current density several orders of magnitude below the remaining traces (11−12% of the total traces recorded for each of the TS samples, and 18−30% of the total traces recorded for each of the AS-DEP samples; see Figure 8a) and (ii) traces directly preceding and following amalgamation (see Figure 8b for the $|J|-V$ signature of amalgamation and Table 3 for the number of times each type of junction failed). The right column of Figure 9 contains the same set of traces for the corresponding AS-DEP junctions. The separation of AS-DEP data into sections "A", "B", and "C" in Figure 9 will aid in the discussion of defect-mediated transport later.

Figure 10 contains histograms of J (bottom, dark gray) and log J (top, light gray), measured at 0.5 V, for the junctions Ag-SC$_n$//C$_n$S-Hg ($n = 10, 12, 14$) using TS silver. It is immediately clear from these plots that J is not normally distributed in any case; for all samples, the peak of the distribution of J lies close to its minimum value. For the TS samples, log J is approximately normally distributed (the peak of the distribution lies close to its median), so we present, as the bold black lines superimposed on the $|J|-V$ curves in Figure 9, a log-mean

(sometimes called a geometric mean),

$$\langle J \rangle_{\log} = 10 \exp\left(\frac{1}{N}\sum_{i=1}^{N}\log_{10}\left|J_i\right|\right) \quad (2a)$$

rather than an arithmetic mean,

$$\langle J \rangle = \frac{1}{N}\sum_{i=1}^{N}J_i \quad (2b)$$

for N values of J at a given voltage. The positions of both means are shown on the histograms. The log−mean lies closer to the peaks of the distributions of values of J than does the arithmetic mean. We do not present averages for the AS-DEP data because it is not meaningful to average data with no identifiable distribution over such a large range.

Figure 11a shows plots of log J (where $J = \langle J \rangle_{\log}$) versus d at the applied voltages $V = 0.05$ and 0.5 V; a linear fit to the TS data yields $\beta = (2.3/d)\log(J_0/J)$. We define d according Figure 11b, where $d \equiv 2(n-1)(1.25\ \text{Å})$. This distance is the sum of the lengths of the *trans*-extended alkyl chains of the molecules that comprise the SAMs on silver and on Hg. The
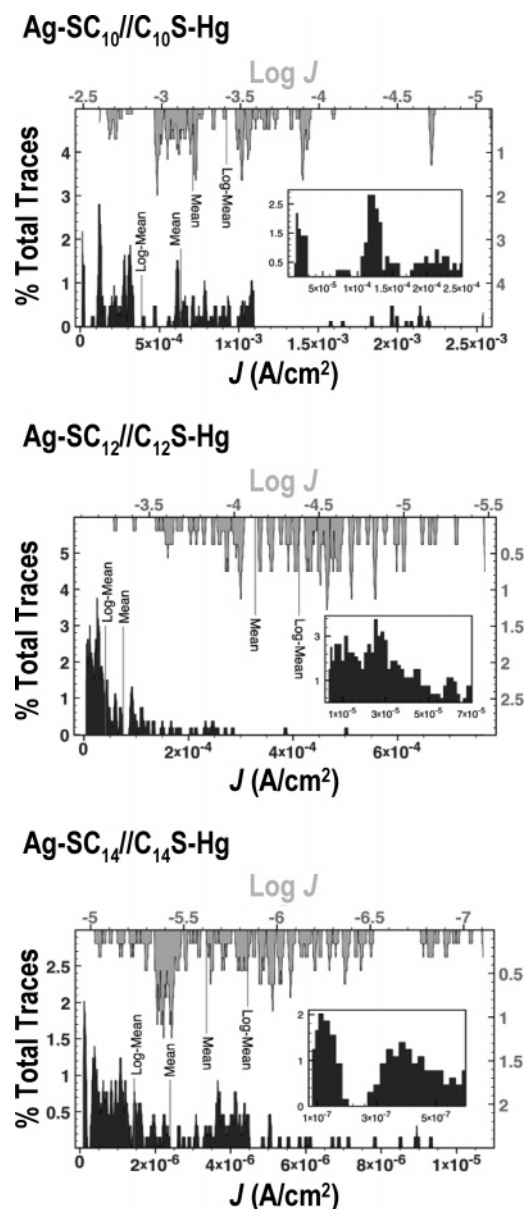
Ag-SC$_{10}$//C$_{10}$S-Hg

Ag-SC$_{12}$//C$_{12}$S-Hg

Ag-SC$_{14}$//C$_{14}$S-Hg

Figure 10. Histograms of the current density (*J*, dark gray, bottom and left axes) and log *J* (light gray, top and right axes) at +0.5 V for the junctions Ag-SC$_n$//C$_n$S-Hg ($n = 10, 12, 14$) using TS silver. The *y*-axis is the percentage of total traces measured at a particular value of *J* or log *J* for the specified type of junction. The arithmetic mean of *J* and the log-mean of *J* are defined in the text (eqs 2a and 2b). The log-mean lies closer to the peaks of the distributions of values of *J* (shown in the insets) than does the arithmetic mean.

trans-extended alkyl chain extends from carbon 1 (C$_1$) to the terminal carbon *n* (C$_n$) along the long molecular axis. In a *trans*-extended alkyl chain, the vector that connects two adjacent carbons—where the C−C bond distance is 1.54 Å—has a projection with magnitude ~1.25 Å along the long axis of the molecule. The fact that log *J* is proportional to *d*—and that log *J* is approximately normally distributed—suggests that *d* may have a normal distribution and, in turn, that inhomogeneous disorder in thickness of the insulating layer is responsible for the variation in *J*.[79]

We chose d_0—the portion of the tunneling barrier that remains constant for $n = 10, 12, 14$—to be the sum of three distances:

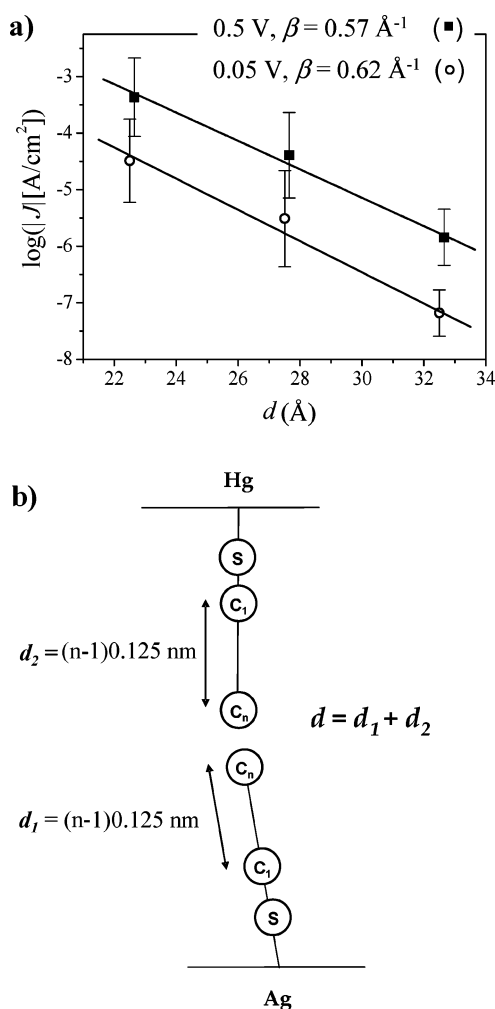(79) Engelkes, V. B.; Beebe, J. M.; Frisbie, C. D. *J. Phys. Chem. B* **2005**, *109*, 16801.

a)

b)

Figure 11. (a) Plots of log *J* vs $d = 2(n − 1)1.25$ Å within the bilayer junctions Ag-SC$_n$//C$_n$S-Hg incorporating TS silver at the applied voltages (○) +0.05 V and (■) +0.5 V. The error bars are the standard deviation of log *J* values for all traces shown in Figure 9 (106 traces for $n = 10$, 76 traces for $n = 12$, 80 traces for $n = 14$). For clarity, the points at $V = 0.5$ V for a given chain length are slightly offset from the points at $V = 0.05$. The lines are the linear least-squares fits of *J*. The slope of these lines (β/2.3) yields $\beta = 0.62$ Å^{-1} for $V = +0.05$ V, and $\beta = 0.57$ Å^{-1} for $V = +0.5$ V. (b) Definition of *d* for an idealized structure of one pair of molecules within a bilayer Ag-SC$_n$//C$_n$S-Hg junction. The alkanethiolate molecule is tilted ~10° on Ag and ~0° on Hg. The distances between C$_1$, the carbon bonded to the sulfur atom (S), and C$_n$, the terminal carbon of the alkyl chain, along the molecular axes of the alkanethiolates on Ag and Hg are given by d_1 and d_2, respectively ($d = d_1 + d_2$). The carbon atoms between C$_1$ and C$_n$ are omitted for clarity.

(i) between the Ag surface and C$_1$ of the attached alkanethiolate molecule, (ii) between the Hg surface and C$_1$ of the attached alkanethiolate molecule, and (iii) between terminal carbons at the van der Waals interface. Our choice of d_0 does not affect the value of β that we extract from the plot of log *J* vs *d* because $\beta = \Delta$ log $J/\Delta d$ (log *J* is determined experimentally, and $\Delta d = 5$ for $n = 10, 12, 14$, i.e., for $d = 22.5, 27.5, 32.5$ Å). Our choice of d_0 does, however, affect the magnitude of J_0: for a given SAM, increasing d_0 decreases *d* and decreases the calculated J_0 (according to eq 1b).

The values of β for the TS surfaces ($\beta = 0.57$ Å^{-1} at +0.5 V and 0.62 Å^{-1} at +0.05 V) are smaller than those measured previously for AS-DEP surfaces (Table 2). In order to explain this disagreement, we again invoke the argument that defects originating from the underlying metal substrate contribute to

the defect-mediated *J* more than do intrinsic defects in AS-DEP junctions, whereas the opposite is true in TS junctions. By this argument, the roughness of the substrate would affect AS-DEP junctions incorporating SAMs of SC_{14} the least, and would affect those incorporating SAMs of SC_{10} the most, because the roughness of the substrate does not translate into disorder in the SAM for SAMs of SC_{14} as much as it does for the more liquid-like SAMs of SC_{10}. Substrate-induced defects include both thin-area and thick-area defects, but, as discussed above, only the thin-area (or high-*J*) defects contribute to the average observed value of *J*. The average value of *J*, therefore, would be *least* inflated from its value through a defect-free SAM for SC_{14} junctions and *most* inflated for the SC_{10} junctions. The observed value for β would, therefore, be larger for a series of AS-DEP junctions than for a series of TS junctions. Intrinsic defects are present in our TS junctions and in the AS-DEP junctions examined in previous work; therefore, the influence of these defects is, in principle, constant for a given chain length from experiment to experiment, regardless of the properties of the substrate. In summary, by using ultraflat surfaces, we reduced the contribution of defects originating from the metal substrate to the average current density; our value for β for the TS junctions is thus lower than previously observed values measured with AS-DEP junctions.

The values for β for the TS junctions are also lower than those measured using two Hg-drop electrodes (0.71 Å^{-1},[54] 0.82 Å^{-1},[52] 1.0 Å^{-1} [49]). By monitoring the evolution of current through and the capacitance of Hg-drop junctions incorporating bilayers of alkanethiolates, Slowinski and Majda[49] concluded that the van der Waals interactions between SAMs on each Hg drop, and the Coulombic forces between the drops themselves, combined to cause disorder in the SAMs (by creating *gauche* defects), intercalate the alkyl chains at the SAM//SAM interface, and eventually collapse the junctions. At times on the order of seconds to minutes, intercalation dominated the behavior of the SC_{16} bilayer junctions, and formation of *gauche* defects dominated the SC_{10} bilayer junctions. The current through SC_{16} junctions was, therefore, artificially high, and the current through the SC_{10} junctions was artificially low; these effects combined to decrease the value of β as the scan rate slowed. While we cannot discount the junction disorder/intercalation explanation for our low value of β, there are three reasons why we do not believe it accounts for our observations. (i) We collected *J*-values after applying a constant bias for 2 s, a time shorter than that needed to induce significant changes in current in the junctions measured by Slowinski and Majda.[49] (ii) Our junctions should be less sensitive to deformation by applied voltage than are the Hg-Hg junctions, because ours have one solid electrode rather than two deformable electrodes. (iii) We applied, at maximum, a voltage of ±0.5 V across the bilayer junction; Slowinski's experiment was performed at a bias of +1.5 V and thus involved higher electrostrictive pressures than ours.

(c) Uncertainty in *J* for TS Junctions. After excluding the initial traces that we have attributed to transport through solvent layers, the range of values of *J* at a given voltage for the TS junctions was about 10^2. The error in estimating the size of the junction contributes to, but does not totally account for, this range. Figure S2 (Supporting Information) plots the area of the junction as a function of the magnified, on-screen image on which we measured the diameter of the junction for the most

commonly used values of magnification (250×, 300×, and 350×). At these magnifications, the measured diameters were usually 6–10 cm on-screen. Even for the case where the area of the junction increases most sharply with measured junction size—a 10-cm junction at 250× magnification—an error in diameter of ±2 cm (from 8 to 12 cm) only yields a range in area of about a factor of 2 (and, therefore, a range in *J* of a factor of 2 because *J* depends linearly on the area of the junction).[80]

One hypothesis to explain the range in *J* of 10^2 for the TS samples is that the lowest-*J* traces in Figure 9—traces that were recorded post-solvent expulsion—represent charge transport through the SAM with the lowest density of defects, and all other traces represent artificially high current density mediated by thin areas of the SAM (see Figures 7 and 8). Assuming the correctness of this hypothesis, and assuming further that the lowest values of *J* in the TS samples occur through essentially defect-free junctions, we estimate that *J*, at +0.5 V, through the defect-free SAM would be 1.2×10^{-4} A/cm² for $n = 10$, 3.0×10^{-5} A/cm² for $n = 12$, and 2.0×10^{-7} A/cm² for $n = 14$. Using these numbers, we obtain $\beta = 0.64$ Å^{-1}—a value that is slightly higher than what we obtained using the log-means of *J*, $\beta = 0.57$ Å^{-1}. This hypothesis is supported by the data in the histograms in Figure 10: the peak of the distribution of *J*-values lies at or near the minimum value of *J* for all three junctions (an observation that is not obvious when looking at the *J*–*V* curves plotted on a log scale in Figure 9).

(d) Uncertainty in *J* for AS-DEP Junctions. The large range of *J*-values (Figure 9) and high rate of failure (Table 3) characteristic of AS-DEP junctions, relative to that of TS junctions, argue very strongly that future measurements of current through organic films should be carried out using TS surfaces.[81] Nonetheless, the data from the AS-DEP samples contain information about mechanisms of failure and about the influence of defects on the distribution of *J*-values; they are also relevant to previous work by us[21] on these junctions. In this section, we attempt to extract and interpret some of the information provided by the AS-DEP junctions.

We make two fundamental assumptions in this section: (i) template-stripped junctions have smaller numbers of defects than do AS-DEP junctions and thus give values of *J* and β closer to those obtained through hypothetical defect-free SAMs than the values obtained with AS-DEP films, and (ii) the defect-mediated current in AS-DEP junctions results from defects in the underlying metal substrate that dominate any intrinsic defects that arise from crystallization of the SAM. We then interpret the data obtained for AS-DEP samples with reference to the TS data. We divide the data for the AS-DEP samples into three sets (see Figure 9): (A) traces in which the values of *J* are substantially *greater* than those for the corresponding TS samples (at the same voltage), (B) traces in which the values of *J* are similar for TS and AS-DEP samples, and (C) traces in which the values of *J* are substantially *less* than for TS samples. Briefly, we suggest that, for the AS-DEP samples, the traces in

(80) We observed no correlation between the area of the junction and the magnitude of the current for the TS junctions, possibly because we varied the area of the junction by no more than a factor of 4 (and usually by only a factor of 2), and there was no guarantee that the distribution of defects within every junction was similar.

(81) We did not attempt to improve the quality of the AS-DEP silver substrates by evaporating them onto mica (rather than Si/SiO₂) or thermally annealing before formation of the SAM.

A are erroneous due to tunneling through thin regions, those in B are reliable, and those in C are largely due to tunneling through regions in which solvent separated the SAMs in the bilayer.

GROUP A. In junctions incorporating Ag surfaces that have step edges or grain boundaries, we have proposed that deformation of the mercury drop leads to expulsion of solvent from these defect sites and to subsequent contact between thin areas of the SAM and the mercury electrode. The expulsion of solvent might occur in stages, such that an increasing area of thin SAM is exposed to the mercury drop as the voltage applied to the junction is repeatedly cycled. (This proposal is related to that offered by Majda[49] for his Hg-SAM//SAM-Hg junctions.) When the exposed thin area is great enough, the current density jumps substantially (by 1 order of magnitude or more), and the junction amalgamates. For AS-DEP surfaces, reaching this critical area for amalgamation often takes fewer cycles than for TS surfaces (see Table 3), because the density of grain boundaries and step edges is higher in the AS-DEP surfaces than in the TS surfaces.

For the Ag-SC_{10}//C_{10}S-Hg junctions, the set of values of J for the TS samples represents an approximate upper limit on the set of values of J for the AS-DEP samples (for this AS-DEP sample in Figure 9, there are very few traces that we group in class A). The range of J for the AS-DEP Ag-SC_{12}//C_{12}S-Hg includes some members of class A, and the Ag-SC_{14}//C_{14}S-Hg junctions includes values several orders of magnitude above and below that for the TS Ag-SC_{14}//C_{14}S-Hg junction. Artificially high current densities are probably mediated by transport through thin areas of the SAM. The absence of traces giving high values of J for the SC_{10} AS-DEP samples can be rationalized by the hypothesis that contact of the Hg-SC_{10} electrode with these thin areas resulted in amalgamation *before* a full scan could be completed. This hypothesis agrees with the higher rate of failure in AS-DEP SC_{10} junctions than in SC_{12} SC_{14} junctions (Table 3). This mechanism of "early failure" is an idiosyncrasy of the Hg-drop system, and early failure would have the curious effect of excluding measurements through thin areas of these junctions. For SC_{14}-containing AS-DEP junctions, we observe values of J both higher and lower than those observed for the (we believe, more interpretable) TS junctions. As we have suggested previously, for SC_{14}, amalgamation did not occur as readily through substrate-induced thin areas as for SC_{10}, because the alkyl chains are longer and more tightly packed—and therefore insulate the silver surface from the mercury more effectively—in the SAM of SC_{14} than in the SAMs of SC_{10} and SC_{12}.

GROUP C. We observed that a substantial fraction (~20% for SC_{10}, ~55% for SC_{12}, and ~24% for SC_{14}) of the values for J through AS-DEP junctions were close to or indistinguishable from the value for an open-circuit (10^3–10^5 smaller than the average values of J for the TS samples), and the traces were hysteretic; we have labeled these traces "C" in Figure 9. Two possible explanations for the observation of the traces in this group are that (i) the low current densities reflect transport through layers of Ag_2O or (ii) solvent and thiol molecules in solution are trapped more readily at the SAM//SAM interface in the AS-DEP samples than in the TS samples because defects in the SAM produce cavities at the interface into which solvent molecules can fit. We favor the latter explanation for two reasons. First, X-ray photoelectron spectra (XPS, Figure S3,

Supporting Information) showed that the TS and AS-DEP samples with SAMs of SC_{16} had similar oxygen content; in addition, we have shown previously[59] that much of the oxygen in the SAMs on AS-DEP silver is due to the presence of *sulfur* oxides, and possibly contamination from adsorbed ethanol and carbon compounds, rather than by Ag_2O or surface "AgO". Second, the magnitude of J and hysteresis of the low-current traces for the AS-DEP junctions are similar to those of the initial low-current traces measured in the TS samples; we have attributed these traces to charge transport through solvent because the magnitude of J through the TS junctions eventually increased as, we suspect, solvent was expelled from the junction.

Conclusions

Measurements of current density through Hg-drop junctions incorporating ultraflat silver, produced using the method of template stripping, are much more reliable (the junctions fail less often, and the distribution of measured values of J is several orders of magnitude smaller) than measurements through junctions incorporating AS-DEP silver. In addition to using ultraflat substrates, performing the measurement under a solution of thiol (of the same chain length as that in the SAMs), and forming a junction with the smallest area experimentally practical, also contribute to the reproducibility of the measurements. The use of this combination of experimental conditions— (i) TS surfaces, (ii) a solvent bath containing thiol, and (iii) small junctions—constitutes a substantial step toward making this class of junctions a useful physical-organic tool with which to investigate electron transport through organic thin films. Furthermore, the importance of these three conditions highlights the role of defects in determining the magnitude of current density through a SAM and the stability of the junction to applied voltage: TS surfaces have a low defect density, thiol molecules in solution are available to "repair" pinholes in the SAM, and junctions with small areas minimize the number of defect sites available either to transmit artificially high tunneling currents or to initiate amalgamation.

The electrical characteristics of the TS junctions lead to five conclusions. (i) Whether we consider the log-mean of J or the value of J at the peak of its distribution to be closest to the current density through a "pristine" SAM, our measurements using Ag-SC_n//C_nS-Hg junctions lie well within the range of values of J recorded on analogous junctions using other methods (see Table 1). (ii) The application of voltage appears to expel solvent from the well-ordered regions of the junction. The regions with defects may either retain some solvent molecules (the result is thick-area defects, which do not contribute significantly to the measured current density) or expel the solvent (the result is thin-area defects, which cause the measurement of artificially high values of J and possibly lead to amalgamation). Future experiments will include measurements of the current as a function of the rate at which the voltage is scanned, in order to prove or disprove the solvent-expulsion hypothesis and to probe the dynamics of the solvent-expulsion process. (iii) The variability of d—the effective thickness of the insulating layer, which we presume to be distributed normally within a single junction and from junction to junction—is probably the source of uncertainty in J. (iv) The values of β we calculated (0.57 Å^{-1} using the log-mean of J, and 0.64 Å^{-1} using the value of J at the maximum of the distribution) are closest to that calculated for the monolayer junctions Ag-SC_nS-

Hg with AS-DEP silver and are significantly smaller than that calculated for the junctions Ag-SC$_n$//C$_{16}$S-Hg with AS-DEP silver ($\beta = 0.87$ Å^{-1}, see Table 2). Values of β measured previously with AS-DEP surfaces might be inflated due to the presence of substrate-induced defects, whose influence scales inversely with the crystallinity of the SAM. (v) We believe that a curious characteristic (in fact, a statistical artifact, albeit a useful one) of the Hg-drop junction is that it will amalgamate when a filament forms or a large enough area of thin SAM contacts the mercury drop. By failing, rather than allowing the passage of high currents, this structure-selective amalgamation filters out some of the influence of defects that would otherwise produce anomalously high values of *J*. Junctions that are more robust than the Hg-drop junction do not incorporate the escape route of amalgamation, so a larger percentage of the current density through these junctions may be mediated by filaments and thin regions of the SAM.

Formation of a SAM on a solid metal electrode, and deposition of a conformal top electrode, is a very practical way to construct an organic thin-film device. In this case, our discussion of defects is extremely relevant. The results of experiments that used CP-AFM and STM (even when compiled into histograms) do not translate readily to the performance of the device because the behavior of a single molecule cannot, in general, be extrapolated to that of a SAM or the bulk. The defects that can be bypassed by techniques like STM and CP-AFM, where the surface is simultaneously imaged and measured, are inescapable in a (relatively) large-area device like the Hg-drop junction. Defects are part of any polycrystalline organic device, and we believe that, as has been done in the semiconductor community for years, the electrical characteristics of these defects should be studied comprehensively in investigations of transport through thin organic films.

Supporting Information Available: Additional experimental details and Figures S1−S3. This material is available free of charge via the Internet at http://pubs.acs.org.

JA0677261